Inter-slice leakage and intra-slice aliasing in simultaneous multi-slice echo-planar images

Carolyn Beth McNabb* [a], Michael Lindner* [a,b], Shan Shen [c], Kou Murayama [a, d], Laura Grace Burgess [a], Tom Johnstone [a, e]

*CM and ML contributed equally to this work.

[a]School of Psychology and Clinical Language Science, University of Reading, Reading, United Kingdom

[b]Centre for Integrative Neuroscience and Neurodynamics, University of Reading, Reading, United Kingdom

[c]Technical Support, University of Reading, Reading, United Kingdom

[d]Research Institute, Kochi University of Technology, Kami, Kochi, Japan

[e]School of Health Sciences, Swinburne University of Technology, Hawthorn, Victoria, Australia

Corresponding author: Dr Carolyn Beth McNabb, School of Psychology and Clinical Language Sciences, University of Reading, Harry Pitt Building, Earley Gate, Reading RG6 7BE, United Kingdom. Email: c.b.mcnabb@reading.ac.uk

Simultaneous multi-slice (SMS; multiband) imaging has become an increasingly popular technique owing to vast improvements in acquisition speed and spatial resolution of echo-planar (EPI) and diffusion-weighted images. However, SMS data are prone to motion sensitivity as well as slice leakage artefacts, which spread signal between simultaneously acquired slices. Here we report on an artefact temporally coinciding with signal fluctuations in the eye and spatially distributed in correspondence with multiband slice acceleration (inter-slice leakage) and parallel imaging (intra-slice leakage) factors. In data collected using commonly used SMS-EPI protocols, we measured the intensity of signal fluctuations (artefact severity) at expected artefact positions. Control positions (outside the expected areas of signal leakage) were additionally specified. We demonstrated a direct relationship between eye movements and artefact severity and showed that time series of seed and artefact regions were highly correlated. Use of split slice-GRAPPA did not appear to mitigate the leakage artefacts. Artefacts from slice leakage were visually obvious in this case due to large signal fluctuations associated with eye movement. Less obvious but potentially serious artefacts would result from any signal, and warrant careful consideration when designing experiments employing SMS-EPI.

Keywords: simultaneous multi-slice, multiband, slice leakage, fMRI, artefact, eye blink

Abbreviations: SMS, simultaneous multi-slice; MB, multiband; EPI, echo-planar imaging; GRAPPA, GeneRalized Autocalibrating Partial Parallel Acquisition; FOV, field of view.

1. Introduction

Simultaneous multi-slice (SMS (Larkman et al., 2001), multi-band; MB) protocols for functional magnetic resonance imaging (fMRI) have substantially reduced the acquisition time of echo-planar imaging (EPI) data (Nunes et al., 2006), increasing temporal and spatial resolution and improving statistical results of functional network analyses (Demetriou et al., 2018; Preibisch et al., 2015). However, SMS data are susceptible to leakage artefacts (Xu et al., 2013), which spread signal between simultaneously acquired slices (Todd et al., 2016) and increase the effects of motion. Although recent methods, such as split slice-GRAPPA (Cauley et al., 2014), have been developed to address these issues, slice leakage artefacts still occur.

The impacts of slice leakage on blood oxygen level-dependent (BOLD) activation are well documented (Cauley et al., 2014; Todd et al., 2016); however leakage effects on other types of signal/noise are less well described. Artefacts caused by non-neuronal factors such as motion, magnetic field and radiofrequency disturbances are important considerations for MRI. However, other than SMS-related increases in motion susceptibility (Kelly et al., 2013), the impact of SMS-related slice leakage on non-neuronal artefacts has not been investigated systematically.

While acquiring resting and task-based SMS data for two recent studies, we observed an unexpected artefact that covered parts of the temporal lobes, frontal pole/cerebral white matter, lateral occipital cortex and precentral/superior frontal gyri in some individual subjects' data. The timing of the artefact coincided with signal fluctuations in the eye and (within the plane of the eye) resembled eye motion artefacts that have been previously described (Chen and Zhu, 1997; Zhang et al., 2011). We hypothesised that the artefact originates in the eye and were able to replicate the artefact in a healthy adult subject by asking them to blink heavily (figure 1 and supplementary material S1). Consequently, the current investigation was conducted to examine the contribution of blinking to SMS-related fMRI artefacts.

The spatial configuration of artefacts was consistent between individuals and coincided with the predicted arrangement based on SMS and GRAPPA (GeneRalized Autocalibrating Partial Parallel Acquisition) parameters used to acquire the data (Todd et al., 2016). We wanted to investigate whether the artefact was replicable across subjects and how the artefact behaved with respect to blinking and non-blinking activity. As a supplement to this work we investigated whether the artefact was limited to the specific SMS sequence and parameters employed in this study or was also observable in other SMS sequences in common use. To test this, we collected EPI data using different reconstruction algorithms and SMS algorithms (Center for Magnetic Resonance Research, University of Minnesota [CMRR (Moeller et al., 2010)] vs Siemens). Intra- (GRAPPA) and inter- (SMS) slice leakage artefacts were identified in most cases. The purpose of this article is to describe and discuss the artefact under each of these conditions.

2. Methods

2.1. Participants and task

Four healthy adult volunteers (3 male, 1 female) participated in this study. The protocol was approved by the University of Reading Research Ethics Committee and each participant provided written informed consent.

Participants were scanned during an eye blinking task (7.5 alternating cycles of 20 s blinking and 20 s rest, total scan time 5 minutes); subjects were asked to perform firm blinks by squeezing their eyelids closed repeatedly to simulate the action taken by participants experiencing dry eyes in the

scanner environment. During the 20 s off period, subjects were instructed to have their eyes open but blink as normal.

2.2. SMS sequence and parameters

All data were acquired on a Siemens MAGNETOM Prisma^{fit} 3T MRI scanner (Siemens, Erlangen, Germany) using the standard vendor-provided 32-channel radiofrequency head coil. Scanning was performed using the Siemens SMS BOLD (two-dimensional (2D) multiband gradient echo EPI (SMS-EPI)) sequence, optimized for the 32-channel coil. Acquisition parameters were as follows: 2 × 2 mm voxels in-plane; 2 mm slice thickness with 0% slice gap; 68 slices; 192 × 192 mm in-plane field-of-view (FOV); repetition time (TR) = 1.5 s; echo time (TE) = 30 ms; phase encode (PE) direction P>>A; effective echo spacing 0.47 ms; GRAPPA 2 in-plane; fat saturation; MB slice acceleration factor MB4.

Additional parameters, including multiband slice acceleration factor 2 (to examine different artefact positions) and PE direction A>>P (to examine the effect of the direction of in-slice signal spread) were also evaluated. As these assessments were secondary to the main objective of the study, data are presented in the supplementary materials.

2.3. Manufacturer vs CMRR sequences and the effects of leak block

Next, we evaluated whether the artefact was unique to the Siemens SMS BOLD sequence or also occurs in other SMS sequences. We compared the MB4 data acquired using the Siemens sequence with MB4 data acquired using the Minnesota CMRR multiband sequence (Moeller et al., 2010; Setsompop et al., 2012; Xu et al., 2013). All parameters for the CMRR sequence were the same as those mentioned above for the Siemens MB4 sequence but with echo spacing 0.32 ms.

The CMRR sequence can utilise the slice-GRAPPA or split slice-GRAPPA approach for k-space reconstruction. Slice-GRAPPA relies strongly on static coil sensitivity profiles when reconstructing data acquired using SMS alone but relies more heavily on contrast information when used in combination with in-plane (GRAPPA) acceleration (Setsompop et al., 2012). This leads to increased signal leakage between simultaneously acquired slices (Cauley et al., 2014). Split slice-GRAPPA (leak block) was developed specifically to address this issue, designed instead to balance the errors arising from intra-slice artefacts and inter-slice signal leakage. This method results in higher total artefact error than slice-GRAPPA but is considered to be less detrimental due to its reduced displacement of detected activation (Cauley et al., 2014). To investigate the implications of each, we employed the CMRR sequence with both options applied.

2.4. Analysis of artefact intensity

Artefact locations were detected using in-house-designed Matlab software (Mathworks, Natick, Massachusetts, USA), MAP4SL (available from: https://github.com/DrMichaelLindner/MAP4SL). Expected artefact locations were determined based on Controlled Aliasing in Parallel Imaging (CAIPI)-related FOV and in-plane GRAPPA shifts associated with the SMS sequence (Todd et al., 2016). A seed (one voxel) was placed in the region of visible artefact nearest to frontal orbital and insular cortices. Slice leakage maps were determined from the MB slice acceleration factor, in-plane GRAPPA factor (GRAPPA 2), and in-plane CAIPI-shift (FOV/3). Within each simultaneously acquired slice, two alias locations were expected: one for the CAIPI shift ((FOV/3)*m) and one for GRAPPA ((FOV/3)*m + FOV/2, where m is the number of simultaneously acquired slices) (Todd et al., 2016). The source of the artefact (label A in figure 2) was then assigned to the mask appearing closest to the eye. An additional set of control regions expected to be unaffected by eye movement were also specified. The first control region was placed halfway between the source (mask A, figure 2) and its GRAPPA region in the P>>A direction. From here, each additional control region was shifted dorsally

((number of slices/MB slice acceleration factor)/2), posteriorly (number of voxels in P>>A direction/(MB slice acceleration factor*2)) and medially (from the source) ((number of slices/MB slice acceleration factor)/2). Only the second and third control regions were used for comparison in this analysis. A circular, 29-voxel, in-plane mask with a radius of 6 voxels centred on each artefact location was created (see figure 2).

In accordance with previous work by (Chen and Zhu, 1997), the intensity of the artefact was evaluated by comparing the volume-to-volume signal fluctuations. These were compared between blinking and non-blinking periods. Within each mask, for each voxel the volume-to-volume signal change was calculated and divided by the maximum volume-to-volume signal change (to give percentage signal change). Mean absolute percentage signal change across all voxels in the mask (29-voxel disk) was determined separately for blinking and non-blinking periods. Then, intensity of the artefact at each mask location was quantified as the difference in mean absolute signal change between blinking and non-blinking periods. In order to further evaluate the relationship between blinking (intensity change in the eye) and artefact production, time series correlations (Pearson's correlation coefficients) were calculated for each pair of voxels in the eye (region A) and remaining masks (i.e. voxel 1 of region A was correlated with voxels 1 through 29 of regions A_g, B, B_g, etc.).

3. Results

Appearance of the artefact corresponded with periods of firm blinking, as shown in figure 3. The artefact appeared at expected locations in both hemispheres, as determined by the slice acceleration factor, CAIPI shift and parallel imaging (GRAPPA) factor. Data for the right hemisphere only are presented below.

Volume-to-volume signal fluctuations (representing the intensity of the artefact within each mask for an individual subject) are shown in the top three plots of figure 4. Mean absolute signal change was greatest during periods of blinking compared with periods of non-blinking for all expected artefact regions but not for control regions (figure 4, bottom). All subjects demonstrated similar patterns of artefact intensity across blinking and non-blinking periods (figure 5).

Evaluating the time series of individual voxels in masked regions, voxels in the eye artefact region (A) demonstrated stronger correlations with those of other artefact regions (B-D and A_g-D_g) compared with control regions (figure 6). Lower correlations in control regions suggest that the artefact is unlikely to be driven solely by head motion associated with blinking. This is further supported by data from the control (eyes closed) condition (see supplementary materials figure S2).

To investigate whether the artefact occurs in other SMS sequences, we used the same blinking task during EPI acquisition with the Minnesota CMRR sequence. CMRR data presented with noticeable voxel blurring in sagittal and axial planes but still displayed noticeable artefact in expected regions. Results for the CMRR sequence with slice-GRAPPA and split slice-GRAPPA reconstruction techniques are shown in figure 7. Split slice-GRAPPA was associated with large intra-slice artefacts. Slice-GRAPPA showed increased artefact intensity in only one artefact location (C_g).

The artefact was not limited to the sequences measured above and was also present in data collected using MB slice acceleration factor MB2 (supplementary materials, figure S3) and PE direction A>>P (supplementary materials, figure S4). Standard motion correction had a limited effect on artefact intensity (supplementary materials, figure S5), as did independent components analysis (ICA)-based motion correction (supplementary materials, figure S6).

4. Discussion

A fundamental limitation of SMS-EPI is the ineffectiveness with which simultaneously acquired slices are separated during reconstruction. Data presented here demonstrate that artefacts caused by blinking leak into simultaneously acquired slices at positions predetermined by the multiband slice acceleration factor and in-plane acceleration factor. Leakage occurs in both Siemens and CMRR SMS sequences and, based on our preliminary findings, appears to be more severe when split slice-GRAPPA k-space reconstruction is used. These findings are supported by previous work demonstrating that multiband slice acceleration leads to aliasing between simultaneously acquired slices (inter-slice leakage) and causes additional in-plane aliasing (intra-slice leakage) when combined with parallel imaging (Cauley et al., 2014; Todd et al., 2016).

Artefact intensity, as measured using absolute signal fluctuations, was lower in data acquired using CMRR sequences. However, visual inspection of raw images revealed similar patterns of artefact leakage (both spatially and temporally) compared with Siemens SMS sequences. Upon examination, CMRR data presented with noticeable voxel blurring in sagittal and axial planes, which may have distorted signal fluctuations by mixing signal with surrounding voxels. Voxel blurring may be a result of phase accumulation (a known limitation of early SMS sequences), though this effect should be ameliorated by the use of blipped-CAIPI (Setsompop et al., 2012).

Split slice-GRAPPA was developed to mitigate the impact of inter-slice leakage (Cauley et al., 2014) and has been shown to reduce the incidence of false positives in data acquired using up to 6 times multiband acceleration in combination with in-plane acceleration (GRAPPA 2) (Todd et al., 2016). Slice-GRAPPA and split slice-GRAPPA employ distinct algorithms to separate simultaneously acquired slices during signal reconstruction. At the expense of increased overall and in-plane aliasing, split slice-GRAPPA reduces inter-slice aliasing and subsequent false positive activation. However, data from the current study suggest that the effect of split slice-GRAPPA on non-neuronal artefact intensity requires further investigation. The effectiveness of using a single-band calibration scan in combination with split slice-GRAPPA (as recommended in http://cni.stanford.edu/updates-for-multiband-reconstruction/) may help to reduce artefact severity and should also be investigated.

SMS data are known to exhibit increased sensitivity to head motion, owing to the combination of short TR (spin history) and parallel imaging (Kelly et al., 2013). Lower signal intensity fluctuations in control regions and weaker correlations between voxels in control and source (eye; region A) locations suggest that head motion alone is not responsible for the artefact reported herein. Standard and ICA-based motion correction results presented in the supplementary materials support this claim.

A full-scale systematic investigation evaluating how each parameter affects the severity of non-neuronal artefact leakage is required. Based on the limited number of experiments included in this study, we cannot make any firm recommendations regarding acquisition of SMS-EPI data. However, suggestions for future studies include 1) adjustment of the PE direction to minimise the impact of leakage from eye motion (signal fluctuations from eye movement will spread along the PE direction (Chen and Zhu, 1997)), 2) adjustment of multiband slice acceleration factor to ensure that areas of interest are not collected simultaneously with regions of high signal variation, and 3) slice or head tilting such that areas associated with high signal variation (such as the eyes) are not included in the FOV. In the meantime, piloting of all SMS-EPI sequences is highly recommended.

SMS improves temporal resolution of fMRI data at the expense of signal leakage between simultaneously acquired slices. Artefacts from slice leakage are overtly apparent in this case due to the large signal fluctuations associated with eye movement; however, more insidious inter- and intra-slice aliasing will result from any signal in the image. Use of split slice-GRAPPA may be effective

for reducing rates of false positive activation but does not appear to mitigate leakage of more severe signal changes. These issues are sufficient to warrant further investigation and should be considered before embarking on research employing SMS-EPI.

Acknowledgements

The study was partly supported by JSPS KAKENHI (15H05401, 16H06406, and 18H01102 to K.M.), F. J. McGuigan Early Career Investigator Prize (to K.M.), and the Leverhulme Trust (RPG-2016-146 and RL-2016-030 to K.M.).

All authors have seen and approved the final version of this manuscript.

References

Cauley, S.F., Polimeni, J.R., Bhat, H., Wang, D., Wald, L.L., Setsompop, K., 2014. Inter-slice Leakage Artifact Reduction Technique for Simultaneous Multi-Slice Acquisitions. Magnetic resonance in medicine : official journal of the Society of Magnetic Resonance in Medicine / Society of Magnetic Resonance in Medicine 72, 93-102.

Chen, W., Zhu, X.-H., 1997. Suppression of physiological eye movement artifacts in functional MRI using slab presaturation. Magnetic Resonance in Medicine 38, 546-550.

Demetriou, L., Kowalczyk, O.S., Tyson, G., Bello, T., Newbould, R.D., Wall, M.B., 2018. A comprehensive evaluation of increasing temporal resolution with multiband-accelerated protocols and effects on statistical outcome measures in fMRI. Neuroimage 176, 404-416.

Kelly, M.E., Duff, E.P., Bijsterbosch, J.D., Voets, N.L., Filippini, N., Moeller, S., Xu, J., Yacoub, E.S., Auerbach, E.J., Ugurbil, K., 2013. An assessment of motion artefacts in multi band EPI for high spatial and temporal resolution resting state fMRI. Proceedings of the ISMRM, Abstract.

Larkman, D.J., Hajnal, J.V., Herlihy, A.H., Coutts, G.A., Young, I.R., Ehnholm, G., 2001. Use of multicoil arrays for separation of signal from multiple slices simultaneously excited. Journal of Magnetic Resonance Imaging 13, 313-317.

Moeller, S., Yacoub, E., Olman, C.A., Auerbach, E., Strupp, J., Harel, N., Uğurbil, K., 2010. Multiband multislice GE-EPI at 7 tesla, with 16-fold acceleration using partial parallel imaging with application to high spatial and temporal whole-brain fMRI. Magnetic Resonance in Medicine 63, 1144-1153.

Nunes, R., Hajnal, J., Golay, X., Larkman, D., 2006. Simultaneous slice excitation and reconstruction for single shot EPI. Proceedings of the 14th annual meeting of ISMRM, Seattle, Washington, USA, p. 293.

Preibisch, C., Castrillon, J., Buhrer, M., Riedl, V., 2015. Evaluation of multiband EPI acquisitions for resting state fMRI. PloS One 10.

Setsompop, K., Gagoski, B.A., Polimeni, J.R., Witzel, T., Wedeen, V.J., Wald, L.L., 2012. Blipped-Controlled Aliasing in Parallel Imaging (blipped-CAIPI) for simultaneous multi-slice EPI with reduced g-factor penalty. Magnetic Resonance in Medicine 67, 1210-1224.

Todd, N., Moeller, S., Auerbach, E.J., Yacoub, E., Flandin, G., Weiskopf, N., 2016. Evaluation of 2D multiband EPI imaging for high-resolution, whole-brain, task-based fMRI studies at 3T: Sensitivity and slice leakage artifacts. Neuroimage 124, 32-42.

Xu, J., Moeller, S., Auerbach, E.J., Strupp, J., Smith, S.M., Feinberg, D.A., Yacoub, E., Uğurbil, K., 2013. Evaluation of slice accelerations using multiband echo planar imaging at 3T. Neuroimage 83, 991-1001.

Zhang, X., Ross, T.J., Jo Salmeron, B., Yang, S., Yang, Y., Stein, E.A., 2011. Single subject task-related BOLD signal artifact in a real-time fMRI feedback paradigm. Human Brain Mapping 32, 592-600.

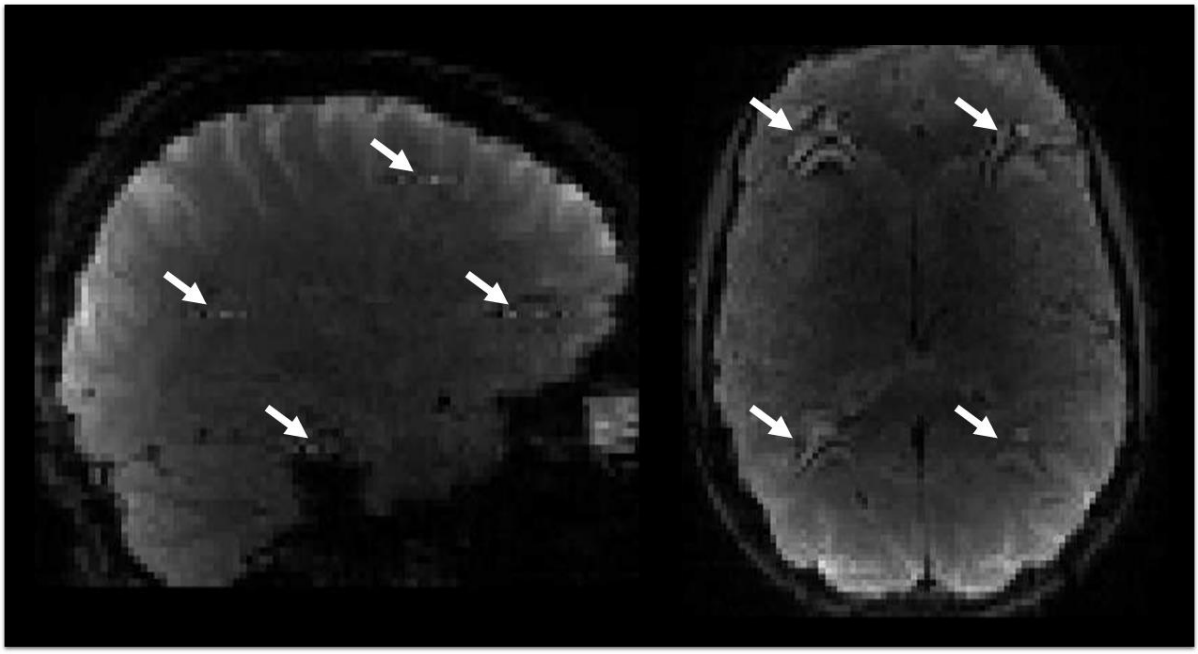

Figure 1. Single volume displaying artefact in individual subject. Dynamic (4 dimensional) time series data are provided in supplementary materials S1.

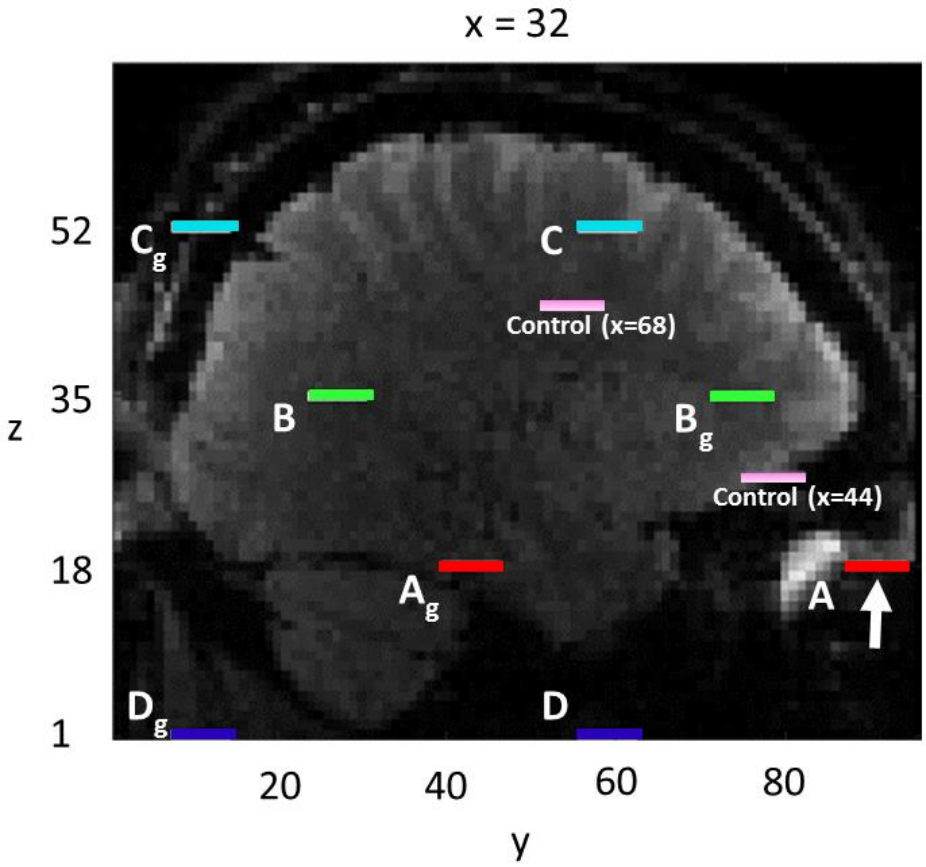

Figure 2. Masks covering expected artefact locations in right hemisphere for an individual subject (centres of expected artefact disks are shown). A-D represent artefact positions expected based on SMS slice acceleration factor (MB4) and CAIPI shift (FOV/3); A_g-D_g represent artefact positions expected based on parallel imaging factor (GRAPPA-2; ((FOV/3)*m + FOV/2), where m is the number of simultaneously acquired slices. Coordinates for artefact source: x=32, y=91, z=18; indicated by white arrow. Control regions are shown in light pink: y and z coordinates are as shown in the figure; x coordinates are specified for each control mask.

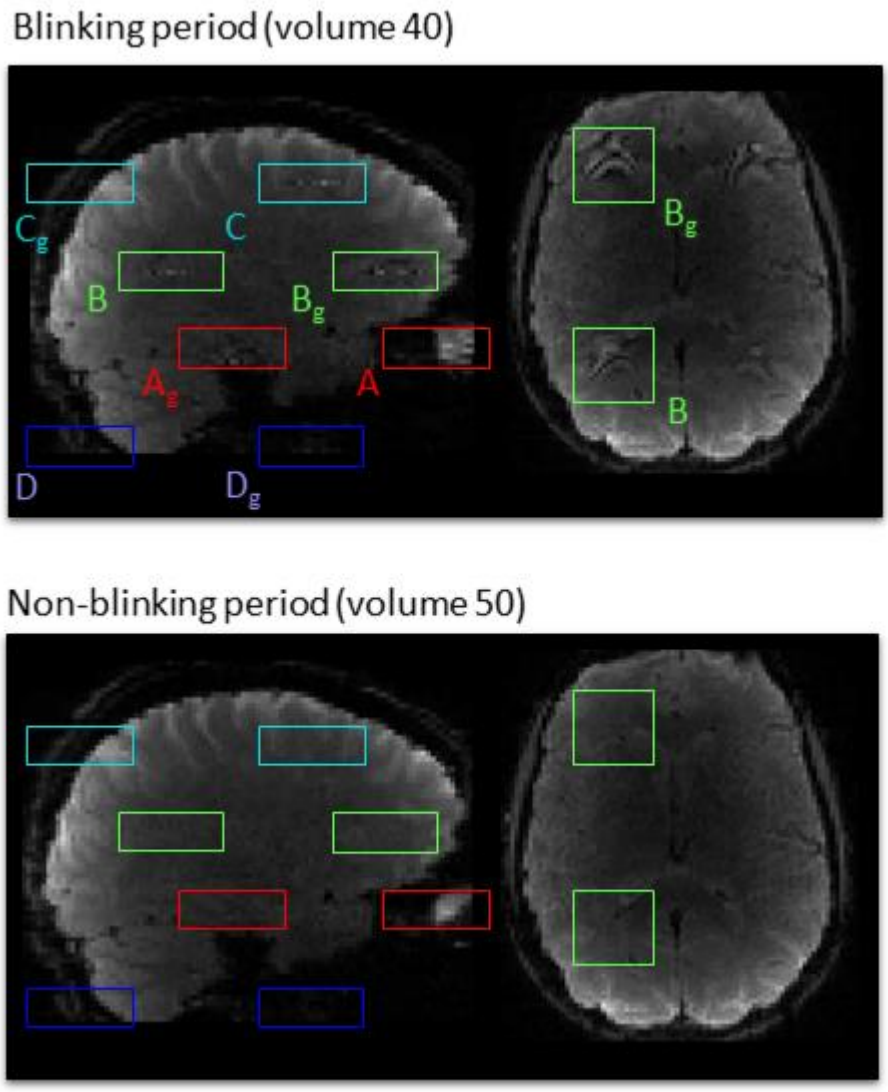

Figure 3. Sagittal and axial slices (x=32) are presented for blinking (top) and non-blinking (bottom) volumes, demonstrating that the artefact is present during blinking but not non-blinking periods. Rectangles highlight artefacts at each expected location (masks were one slice thick).

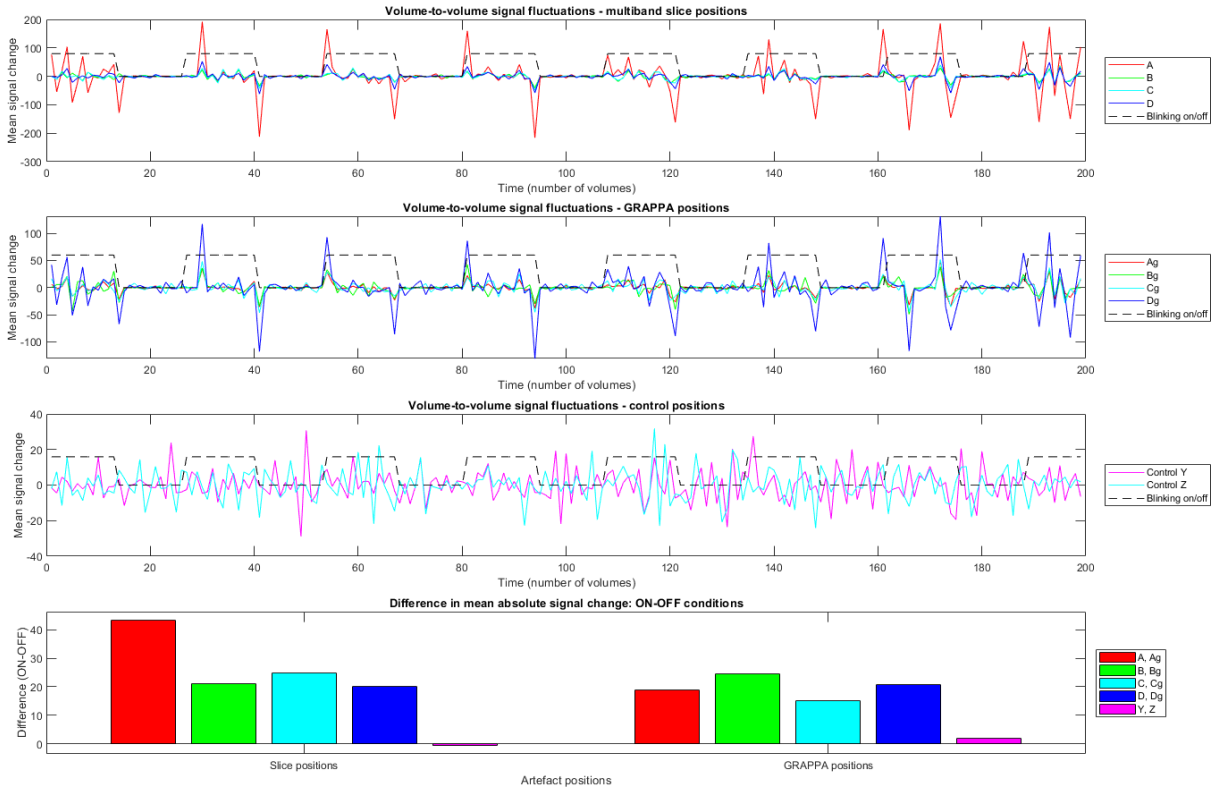

Figure 4. Mean signal change across time within voxels of expected artefact regions and control regions for a single subject (right hemisphere; same subject as for figures 2 and 3) (top 3 plots) and difference in mean absolute signal change between blinking (on) and non-blinking (off) conditions for each respective mask (bottom plot).

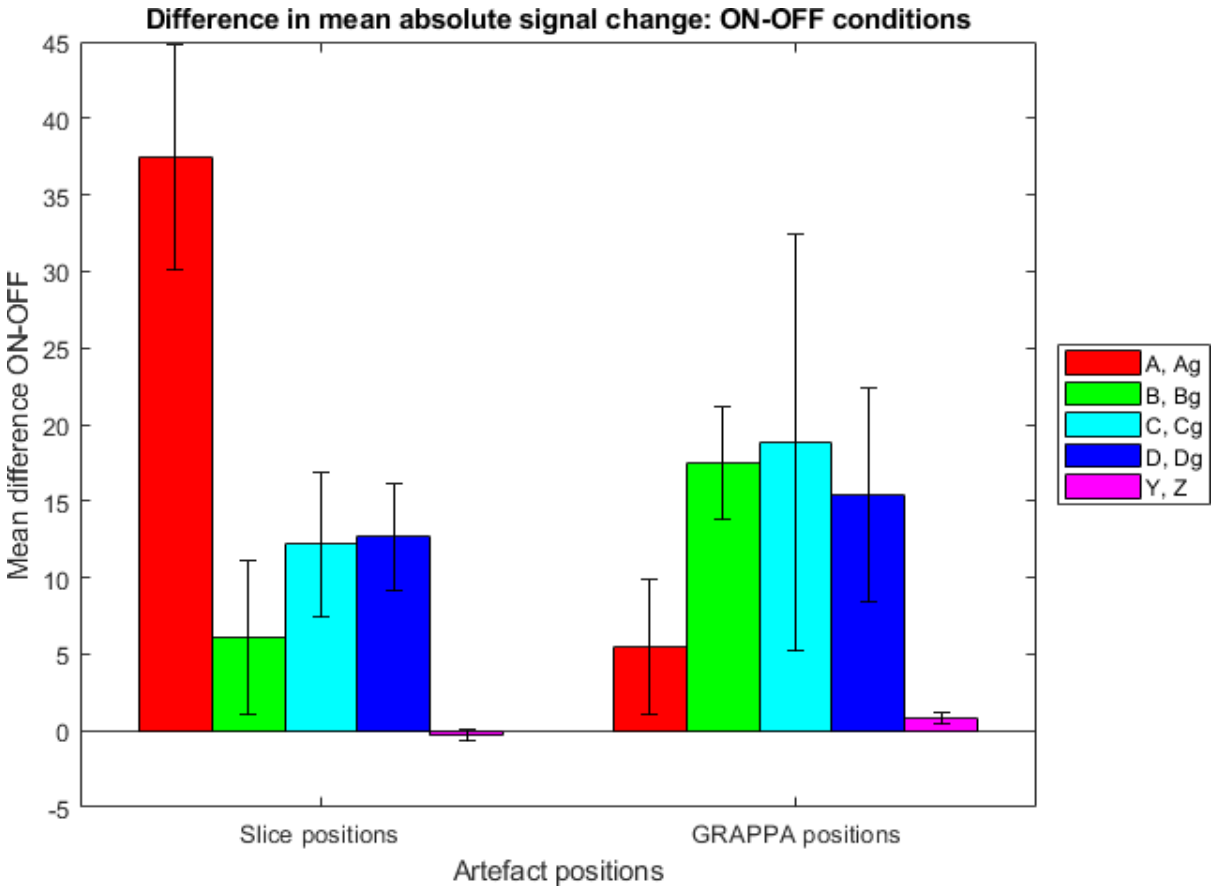

Figure 5. Mean difference (±standard error of the mean; SEM, n=4 subjects) in mean absolute signal change between blinking (on) and non-blinking (off) conditions. Data are shown for expected artefact and control regions (right hemisphere).

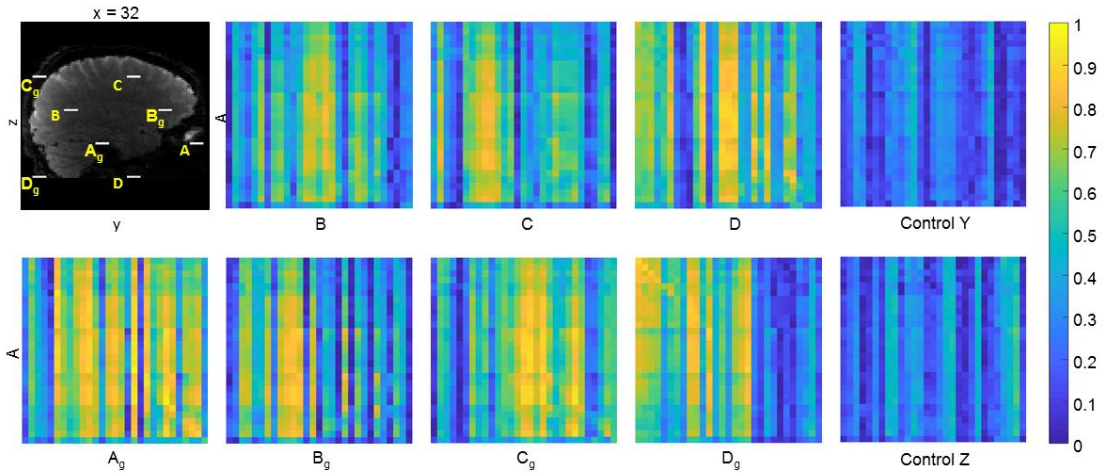

Figure 6. Pearson's correlation coefficients for voxel-by-voxel correlations (absolute r) between region A and remaining artefact (B-D and A_g-D_g) and control (X and Y) regions. Strength of absolute correlations is represented by the colour bar on the right. Data are presented for the right hemisphere for the same subject as earlier figures.

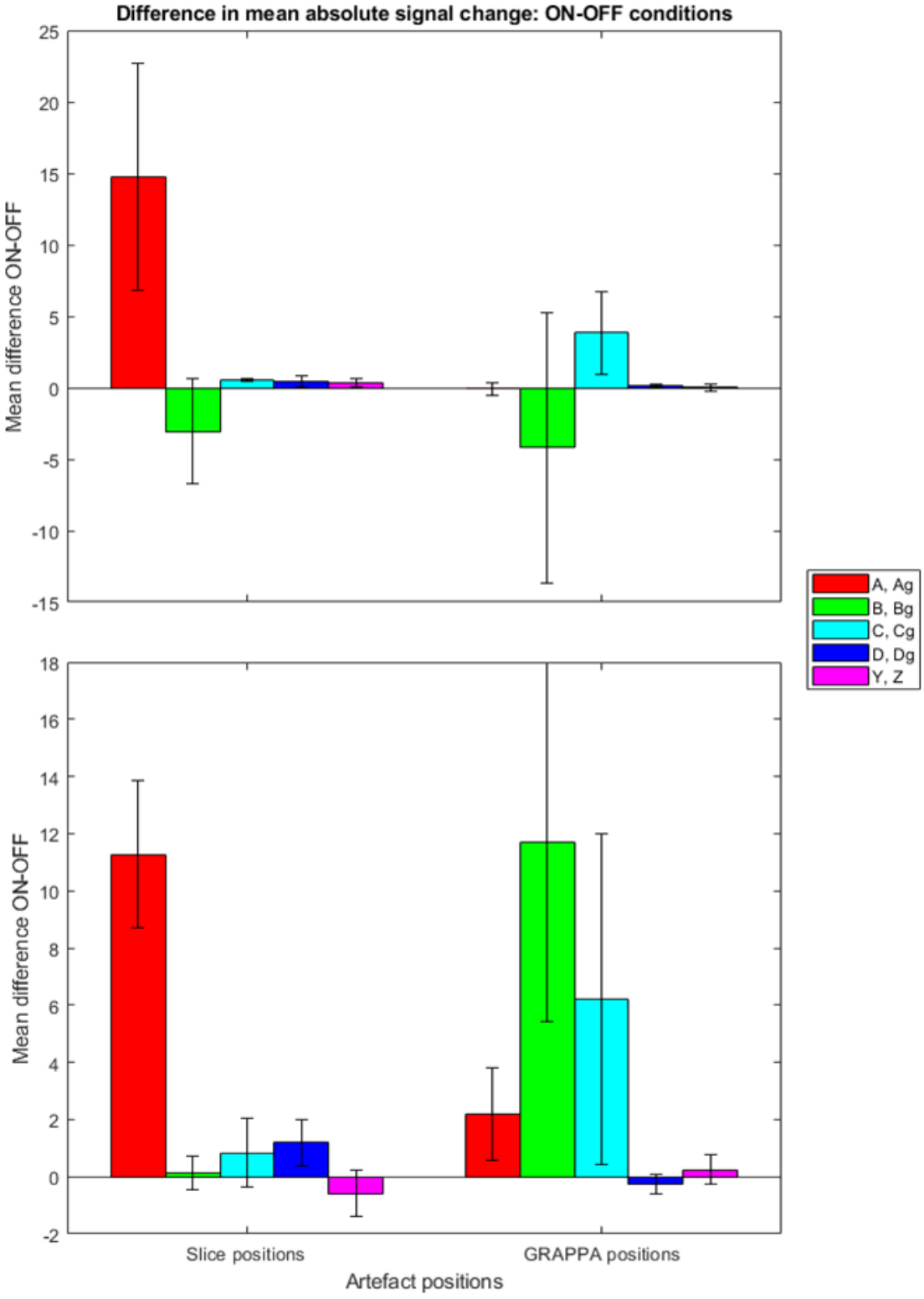

Figure 7. Mean difference (±SEM, n=4 subjects) across subjects in mean absolute signal change between blinking on and off periods for expected artefact and control regions (right hemisphere) for the CMRR sequence using slice-GRAPPA (top) and split slice-GRAPPA (bottom).